

Investigating IceCube Neutrino Alerts with the HAWC  $\gamma$ -Ray Observatory.

R. ALFARO,<sup>1</sup> C. ALVAREZ,<sup>2</sup> A. ANDRÉS,<sup>3</sup> E. ANITA-RANGEL,<sup>3</sup> M. ARAYA ,<sup>4</sup> J.C. ARTEAGA-VELÁZQUEZ ,<sup>5</sup>  
 D. AVILA ROJAS ,<sup>3</sup> H.A. AYALA SOLARES ,<sup>6</sup> R. BABU ,<sup>7</sup> E. BELMONT-MORENO ,<sup>1</sup> A. BERNAL,<sup>3</sup>  
 K.S. CABALLERO-MORA ,<sup>2</sup> T. CAPISTRÁN ,<sup>8</sup> F. CARREÓN,<sup>3</sup> S. CASANOVA ,<sup>9</sup> J. COTZOMI ,<sup>10</sup>  
 S. COUTIÑO DE LEÓN ,<sup>11</sup> C. DE LEÓN ,<sup>12</sup> E. DE LA FUENTE ,<sup>13</sup> P. DESIATI,<sup>14</sup> N. DI LALLA ,<sup>15</sup>  
 R. DIAZ HERNANDEZ,<sup>8</sup> M.A. DUVERNOIS ,<sup>14</sup> J.C. DÍAZ-VÉLEZ ,<sup>14</sup> K. ENGEL ,<sup>16</sup> C. ESPINOZA ,<sup>1</sup> N. FRAIJA ,<sup>3</sup>  
 S. FRAIJA,<sup>3</sup> A. GALVÁN-GÁMEZ,<sup>1</sup> J.A. GARCÍA-GONZÁLEZ ,<sup>17</sup> F. GARFIAS ,<sup>3</sup> N. GHOSH,<sup>18</sup> A. GONZALEZ MUÑOZ,<sup>1</sup>  
 M.M. GONZÁLEZ,<sup>3</sup> J.A. GONZÁLEZ,<sup>5</sup> J.A. GOODMAN ,<sup>16</sup> D. GUEVEL ,<sup>18</sup> J. GYEONG,<sup>19</sup> J.P. HARDING ,<sup>20</sup>  
 S. HERNÁNDEZ-CADENA,<sup>21</sup> I. HERZOG ,<sup>7</sup> J. HINTON ,<sup>22</sup> D. HUANG ,<sup>23</sup> F. HUEYOTL-ZAHUANTITLA ,<sup>2</sup>  
 P. HÜNTEMEYER ,<sup>18</sup> A. IRIARTE ,<sup>3</sup> S. KAUFMANN,<sup>24</sup> D. KIEDA ,<sup>25</sup> K. LEAVITT,<sup>18</sup> J. LEE ,<sup>26</sup> W.H. LEE ,<sup>3</sup>  
 H. LEÓN VARGAS ,<sup>1</sup> J.T. LINNEMANN ,<sup>7</sup> A.L. LONGINOTTI ,<sup>3</sup> G. LUIS-RAYA ,<sup>24</sup> K. MALONE ,<sup>20</sup> O. MARTINEZ ,<sup>10</sup>  
 J. MARTÍNEZ-CASTRO ,<sup>27</sup> J.A. MATTHEWS ,<sup>28</sup> P. MIRANDA-ROMAGNOLI ,<sup>29</sup> P.E. MIRÓN-ENRIQUEZ,<sup>3</sup> E. MORENO ,<sup>10</sup>  
 M. MOSTAFÁ ,<sup>6</sup> M. NAJAFI,<sup>18</sup> A. NAYERHODA ,<sup>9</sup> L. NELLEN ,<sup>30</sup> M.U. NISA ,<sup>7</sup> R. NORIEGA-PAPAQUI ,<sup>29</sup>  
 N. OMODEI ,<sup>15</sup> M. OSORIO-ARCHILA,<sup>3</sup> E. PONCE,<sup>10</sup> Y. PÉREZ ARAUJO ,<sup>1</sup> E.G. PÉREZ-PÉREZ ,<sup>24</sup> C.D. RHO ,<sup>19</sup>  
 D. ROSA-GONZÁLEZ ,<sup>8</sup> M. ROTH ,<sup>20</sup> H. SALAZAR,<sup>10</sup> D. SALAZAR-GALLEGOS,<sup>7</sup> A. SANDOVAL ,<sup>1</sup> M. SCHNEIDER ,<sup>16</sup>  
 J. SERNA-FRANCO,<sup>1</sup> M. SHIN,<sup>19</sup> A.J. SMITH ,<sup>16</sup> Y. SON,<sup>26</sup> R.W. SPRINGER ,<sup>25</sup> O. TIBOLLA,<sup>24</sup> K. TOLLEFSON ,<sup>7</sup>  
 I. TORRES ,<sup>8</sup> R. TORRES-ESCOBEDO ,<sup>21</sup> E. VARELA ,<sup>10</sup> L. VILLASEÑOR ,<sup>10</sup> X. WANG ,<sup>31</sup> Z. WANG,<sup>31</sup>  
 I.J. WATSON ,<sup>26</sup> H. WU ,<sup>14</sup> S. YU ,<sup>32</sup> AND H. ZHOU ,<sup>21</sup>

THE HAWC COLLABORATION

<sup>1</sup> Instituto de Física, Universidad Nacional Autónoma de México, Ciudad de Mexico, Mexico<sup>2</sup> Universidad Autónoma de Chiapas, Tuxtla Gutiérrez, Chiapas, México<sup>3</sup> Instituto de Astronomía, Universidad Nacional Autónoma de México, Ciudad de Mexico, Mexico<sup>4</sup> Universidad de Costa Rica, San José 2060, Costa Rica<sup>5</sup> Universidad Michoacana de San Nicolás de Hidalgo, Morelia, Mexico<sup>6</sup> Temple University, Department of Physics, 1925 N. 12th Street, Philadelphia, PA 19122, USA<sup>7</sup> Department of Physics and Astronomy, Michigan State University, East Lansing, MI, USA<sup>8</sup> Instituto Nacional de Astrofísica, Óptica y Electrónica, Puebla, Mexico<sup>9</sup> Institute of Nuclear Physics Polish Academy of Sciences, PL-31342 IFJ-PAN, Krakow, Poland<sup>10</sup> Facultad de Ciencias Físico Matemáticas, Benemérita Universidad Autónoma de Puebla, Puebla, Mexico<sup>11</sup> Instituto de Física Corpuscular, CSIC, Universitat de València, E-46980, Paterna, Valencia, Spain<sup>12</sup> Instituto de Física Corpuscular, CSIC, Universitat de València, E-46980, Paterna, Valencia, Spain<sup>13</sup> Departamento de Física, Centro Universitario de Ciencias Exactas e Ingenierías, Universidad de Guadalajara, Guadalajara, Mexico<sup>14</sup> Dept. of Physics and Wisconsin IceCube Particle Astrophysics Center, University of Wisconsin—Madison, Madison, WI, USA<sup>15</sup> Department of Physics, Stanford University: Stanford, CA 94305-4060, USA<sup>16</sup> Department of Physics, University of Maryland, College Park, MD, USA<sup>17</sup> Tecnológico de Monterrey, Escuela de Ingeniería y Ciencias, Ave. Eugenio Garza Sada 2501, Monterrey, N.L., Mexico, 64849<sup>18</sup> Department of Physics, Michigan Technological University, Houghton, MI, USA<sup>19</sup> Department of Physics, Sungkyunkwan University, Suwon 16419, South Korea<sup>20</sup> Los Alamos National Laboratory, Los Alamos, NM, USA<sup>21</sup> Tsung-Dao Lee Institute & School of Physics and Astronomy, Shanghai Jiao Tong University, 800 Dongchuan Rd, Shanghai, SH 200240, China<sup>22</sup> Max-Planck Institute for Nuclear Physics, 69117 Heidelberg, Germany<sup>23</sup> Department of Physics and Astronomy, University of Delaware, Newark, DE, USA<sup>24</sup> Universidad Politécnica de Pachuca, Pachuca, Hgo, Mexico<sup>25</sup> Department of Physics and Astronomy, University of Utah, Salt Lake City, UT, USA<sup>26</sup> University of Seoul, Seoul, Rep. of Korea<sup>27</sup> Centro de Investigación en Computación, Instituto Politécnico Nacional, México City, México.<sup>28</sup> Dept of Physics and Astronomy, University of New Mexico, Albuquerque, NM, USA

<sup>29</sup>Universidad Autónoma del Estado de Hidalgo, Pachuca, Mexico

<sup>30</sup>Instituto de Ciencias Nucleares, Universidad Nacional Autónoma de Mexico, Ciudad de Mexico, Mexico

<sup>31</sup>Department of Physics, Missouri University of Science and Technology, Rolla, MO, US

<sup>32</sup>Department of Physics, Pennsylvania State University, University Park, PA, USA

## ABSTRACT

Neutrino emission from astrophysical sources has long been considered a signature of cosmic-ray acceleration. The IceCube neutrino observatory has observed a diffuse flux of TeV-PeV neutrinos, but very few confirmed sources have emerged. With the recent publication of IceCube Event Catalog (IceCat-1), IceCube has released a list of the most promising astrophysical neutrino events since May 2011. Using the archival data from the High Altitude Water Cherenkov (HAWC)  $\gamma$ -ray observatory, we perform a coincidence search for gamma rays and neutrinos using a Bayesian Block algorithm with the public IceCube alerts from IceCat-1, along with additional alerts issued later. In this work, we consider 368 alerts, up to July 8, 2025, that are within HAWC’s field of view. We observe approximately a 5% coincident detection rate, which is consistent with expectations from background. Two of these detections contain the Active Galactic Nuclei (AGN) Markarian 421 and Markarian 501. We discuss the likelihood that the neutrino/ $\gamma$ -ray coincidences are false positives and a brief overview of the results.

**Keywords:** High energy astrophysics (739) — Active galactic nuclei (16) — Gamma-ray astronomy (628) — Neutrino astronomy (1100)

## 1. INTRODUCTION

Multi-messenger astronomy has become essential for connecting observations across the electromagnetic (EM) spectrum with signals from gravitational waves and particles like neutrinos. Specifically, studies in the TeV range can help place limits on particle energies and offer clues about the underlying acceleration mechanisms of ultra high-energy cosmic rays. Multi-wavelength observations of events like the joint EM and gravitational wave observations of GW150914 (B. P. Abbott et al. 2016) and the neutrino and EM flaring of TXS 0506+056 (M. G. Aartsen et al. 2018), along with their extensive follow-up observations, have significantly improved our understanding of the physics of extremely energetic environments.

In particular, coincident neutrino and  $\gamma$ -ray emission can be used to place constraints or determine the origin of the most energetic cosmic rays. In the TeV regime,  $\gamma$ -rays are produced one of two ways: either through the inverse Compton scattering of leptons or pion decay in hadronic interactions (F. A. Aharonian 2004). Crucially, pion decay produces neutrinos in addition to  $\gamma$ -rays. Therefore, observing joint neutrino and TeV  $\gamma$ -ray emission from sources would provide conclusive evidence about the nature of a particular  $\gamma$ -ray source.

There have been few neutrino sources identified as of writing. The IceCube neutrino observatory (further discussed in Section 2.2), is sensitive to TeV-PeV neutrinos and has recently observed diffuse neutrino emission from the galactic plane (R. Abbasi et al. 2023a) along with a

few extragalactic sources. These include Active Galactic Nuclei (AGN) like TXS 0506+056 (M. G. Aartsen et al. 2018) and NGC 1068 (R. Abbasi et al. 2022).

Additionally, the IceCube observatory sends out public alerts for probable astrophysical neutrinos. Archival versions of these alerts were published as IceCat-1 (R. Abbasi et al. 2023b) and current alerts are distributed via the Astrophysical Multimessenger Observatory Network (AMON) (H. A. A. Solares 2019) and NASA’s General Coordinate Network (GCN). These can be found on AMON’s website <sup>33</sup>. Further details are discussed in Section 3.

As for TeV  $\gamma$ -ray emission, current observatories like the High Altitude Water Cherenkov (HAWC) Gamma-ray Observatory (A. Abeysekara et al. 2023a), the Large High Altitude Air Shower Observatory (LHAASO) (Z. Cao et al. 2019), and future observatories like the Southern Wide-field Gamma-ray Observatory (SWGO) (P. Abreu et al. 2019) are ideally suited for observing both steady-state and transient sources. HAWC has observed the two flaring AGN Markarians (Mrks) 421 and 501 (A. Albert et al. 2022) along with several other AGN (R. Alfarro et al. 2025a). Additionally, HAWC is sensitive to transient events (A. Abeysekara et al. 2017) and can be used to follow up any alerts sent by IceCube.

In this paper, we search for temporal flaring of  $\gamma$ -rays at the locations of IceCube alerts in archival HAWC

<sup>33</sup> [https://gcn.gsfc.nasa.gov/amon\\_icecube\\_gold\\_bronze\\_events.html](https://gcn.gsfc.nasa.gov/amon_icecube_gold_bronze_events.html)

data. First, we introduce both the HAWC  $\gamma$ -ray and IceCube neutrino observatories (Section 2) and describe the data that are used from both of them in this analysis (Section 3). In Section 4, we discuss HAWC’s data collection method and introduce the fitting algorithm: the Bayesian Block algorithm. The results of applying this algorithm to HAWC’s data are presented in Section 5. Next, a multi-messenger interpretation of the observed neutrino/ $\gamma$ -ray coincidences is presented in Section 6. All results are then further discussed in Section 7.

## 2. OBSERVATORIES

### 2.1. HAWC

HAWC is located on the slopes of the Sierra Negra volcano in Mexico, at an altitude of about 4,100 meters. It is composed of 300 large water tanks, each equipped with photomultiplier tubes (PMTs) at the bottom to detect Cherenkov light generated by secondary particles from gamma-ray air showers. The main array contains 1,200 PMTs spread across the tanks, enabling a wide Field of View (FOV). HAWC observes gamma rays in the energy range from about 300 GeV up to beyond 100 TeV. With an uptime of 93% and 2 sr FOV, it is ideal for capturing high energy transient  $\gamma$ -ray events (A. Abeysekara et al. 2023b).

### 2.2. IceCube

The IceCube Neutrino Observatory, located at the South Pole, is a cubic-kilometer-scale detector embedded deep within the Antarctic ice. It consists of three main components: the in-ice array, IceTop (a surface air-shower array), and DeepCore (a denser sub-array for lower-energy neutrinos). The in-ice array is made up of 86 vertical strings, each instrumented with Digital Optical Modules (DOMs), totaling 5,160 DOMs that detect the Cherenkov light produced when neutrinos interact with the ice. IceCube is sensitive to a broad energy range, from roughly 10 GeV with DeepCore up to beyond 1 PeV, and with an uptime of  $> 99\%$  and a 360 degree FOV, it is ideal for capturing transient neutrino events (M. G. Aartsen et al. 2017).

## 3. DATA

The IceCube neutrino data considered are astrophysical neutrino alerts from R. Abbasi et al. (2023b) from 2011 to 2022 and the public alerts distributed via GCN onwards. This analysis considers alerts up to July 8, 2025, with 368 alerts in HAWC’s FOV. The alerts contain the alert name, time, location (including 95% containment), energy, and probability of being astrophysical. They are split into two categories: bronze if the probability is  $\geq 30\%$  and gold if the probability is

$\geq 50\%$ . These are indicated by either B or G, respectively. Lastly, IceCube’s Point Spread Function (PSF) quite variable depending on the alert, ranging from  $>10$  to  $<0.2$  degrees.

For HAWC data, two data sets are considered: the full time-integrated Pass 5 data set containing 2565 full days of reconstructed data, discussed in A. Albert et al. (2024), and individual daily maps. These daily maps utilize the same reconstruction method as the Pass 5 data set and run from March 20, 2015 to January 15, 2024. Temporal coincidences are searched for within this range, with locational coincidences outside HAWC’s operation period also considered. Accounting for detector downtime (complete power down), there are 3175 days of potential data, though in practice that number is lower depending on what IceCube alert is considered. This is due to detector events like small-scale maintenance or high electric field events that may affect the data collection of HAWC for part of the day. It should be noted that the Pass 5 data set takes this into account and excludes those days, while the daily maps do not. This explains the difference in days in the respective data sets. The implications of this are discussed in Section 7. The full data set is used to search for potential neutrino coincidences with HAWC steady-state sources while the daily maps can search for transient events like potential flares. All the IceCube alerts visible to HAWC are shown in Figure 1. Like with IceCube, HAWC’s PSF is dependent on the events observed and can range from  $>1$  to  $\approx 0.1$  degrees for lower and higher energy events, respectively.

HAWC utilizes three different techniques to reconstruct its data. Discussed in A. Albert et al. (2024), these are the  $f_{hit}$ , Neural Network (NN), and Ground Parameter (GP) maps. In brief, the  $f_{hit}$  dataset is constructed by recording the fraction of PMTs triggered by an air shower and is good for low to medium energy events (0.3 to  $\approx 10$  TeV), but then the detector becomes saturated and triggers all PMTs, making accurate energy estimation difficult. The NN and GP are both energy estimators that span HAWC’s full energy range (0.3 to  $> 100$  TeV). The NN uses primarily the fractional charge distribution of nine concentric annuli around a shower core to reconstruct the principle energy. HAWC’s daily maps utilize the  $f_{hit}$  estimator while the reconstructed data set makes three separate maps, one for each estimator. The  $f_{hit}$  and NN maps are presented in this work, while the GP was used to validation.

When creating HAWC’s significance maps, a likelihood test is performed by defining a test statistic (TS) that is the ratio of an alternate hypothesis (background

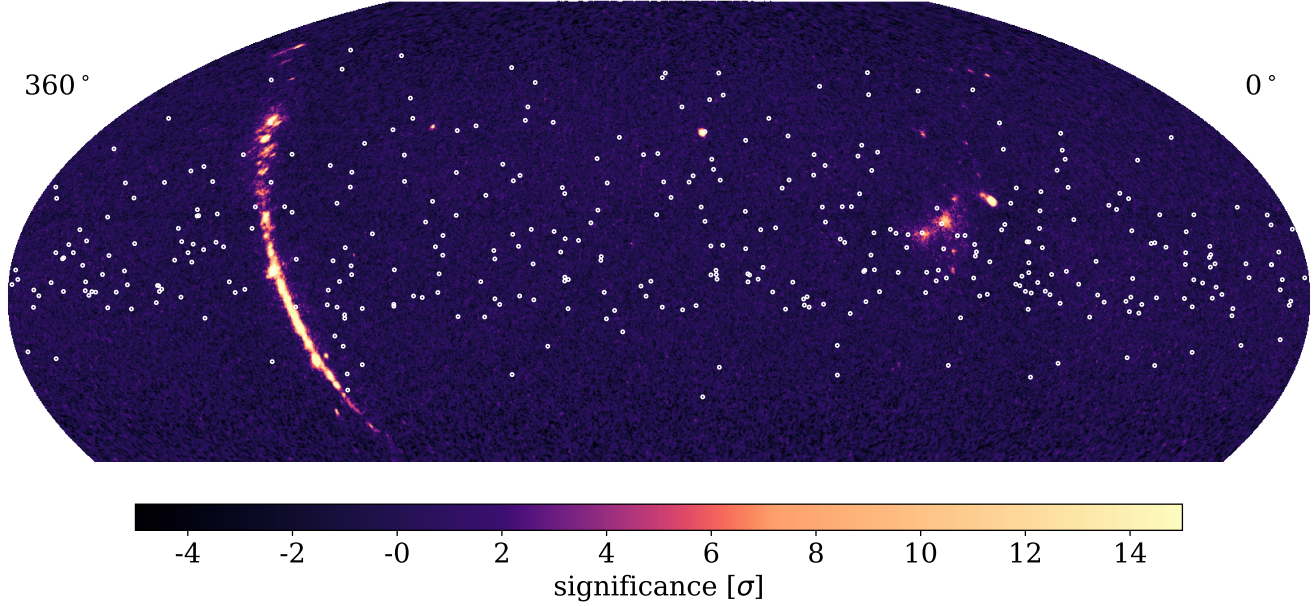


**Figure 1.** HAWC’s full sky data map with the 368 visible IceCube alerts. The white dots show the alerts that lie within the declination interval  $-20^\circ$  to  $60^\circ$ . This range is selected to constrain large IceCube alerts and prevent the ROI from extending beyond HAWC’s FOV. The plot is drawn in celestial coordinates with an index of 2.7 and a pivot energy ( $E_p$ ) of 7 TeV.

+ source) and null hypothesis (background only). The TS is defined as

$$TS = 2 \ln \frac{L_{alt}}{L_{null}}. \quad (1)$$

Assuming Wilks’ theorem (S. S. Wilks 1938), if the difference in free parameters between the two models is one, then the TS is distributed as a  $\chi^2$  distribution with the degrees of freedom equal to the number of free parameters and the significance in deviation between the two models can be approximated as  $\sigma = \sqrt{TS}$ .

The spectral assumption used for the model discussed above is a simple power law, given by

$$\frac{dE}{dN} = N_o \left( \frac{E}{E_p} \right)^{-\alpha}, \quad (2)$$

where  $N_o$  is the flux normalization,  $\alpha$  is the spectral index, and  $E_p = 7$  TeV is the pivot energy. We created two maps with fixed indices 2.0 and 3.0, allowing only the flux normalization to float. These favor either harder indices/higher energy or softer indices/lower energy events, respectively. Henceforth, these maps will be referred to 2.0 or 3.0 maps.

## 4. METHODOLOGY

### 4.1. Data Collection

Searching the HAWC data using the IceCube alerts is done as follows: first, the location and uncertainty region from each alert is extracted and used to construct a Region of Interest (ROI). Then, the time integrated HAWC data set is scanned to find the brightest significance spot inside the ROI to determine if a steady  $\gamma$ -ray source is present. If there is no data contained with IceCube alert for a given day due to a partial map, it receives a null entry and moves to the next day. These results are used to draw potential correlations between the alerts and known HAWC sources, and are discussed further in Section 6.

Next, both the 2.0 and 3.0 daily map sets are considered. For each day, the pixels in the data maps within the ROI are scanned to search for the pixel with the maximum flux value, corresponding uncertainty and its location (RA, DEC). If a flare (event above background) is present and visible to HAWC, its flux would appear above the background for the given day. The fluxes and uncertainties are extracted, and then a light curve is made for the ROI. The TeV-bright AGN Mrk 421 is located 0.8 degrees from the neutrino alert IC111208B and used as an example for this procedure. Example signifi-

cance maps and resulting maximum flux distribution are shown in Figure 2.

#### 4.2. Bayesian Block Algorithm (BBA)

While extraordinarily bright transient sources like Mrk 421 can be found easily by eye, most sources are too dim to do this. Therefore, we apply the Bayesian Block Algorithm (BBA), mathematically described in J. D. Scargle et al. (2013), and use the code implementation from S. M. Wagner et al. (2021). A brief description of the BBA is presented here. The goal of the BBA is to find statistically significant deviations in data. We use it in its “piecewise function” model with the algorithm set in the “Point Measurements” setting (see Section 3.3 in J. D. Scargle et al. (2013)). The blocks are described by step functions with 0 slope across a certain interval determined by the sensitivity of the algorithm and the data is defined by time-independent (1 value per time step) values with some uncertainty. The start and end points for the blocks are called “change points”, where the minimum number of change points is 2 for one block. We consider the number of change points above this minimum, dubbed  $n_{cp}$ , which is the total number of change points minus 2.

To determine the total number of blocks for a given data set, a global “fitness function” is defined as

$$F[P(T)] = \sum_{k=1}^{N_{blocks}} f(B_k), \quad (3)$$

where the global fitness function for a given partition of the data  $P(T)$  is the sum of each block’s fitness functions  $B_k$ . If we assume a steady-state emission model  $\lambda = s$ , with  $\lambda$  being the model and  $s$  some constant value, and a normal distribution with zero mean and a known variance for the observational error, the individual block fitness functions become a log likelihood function of form

$$\log L_{\max}^k = \sum_n \frac{x_n^2}{\sigma_n^2}. \quad (4)$$

The block’s fitness function is only dependent on what data and uncertainty  $x_n \pm \sigma_n$  is included inside it and is time-independent. To prevent overfitting, a penalty factor is included to penalize models with more blocks. The new global fitness function now becomes

$$F[P(T)] = \sum_{k=1}^{N_{blocks}} \left( \sum_n \frac{x_n^2}{\sigma_n^2} \right) - N_{blocks} \log \gamma, \quad (5)$$

with  $-\log \gamma$ , also called the  $ncp\_prior$ , being the penalty factor and which is a tunable parameter. The  $ncp\_prior$  determines how sensitive the BBA is to deviations in

the data. If it is too small, the BBA will fit blocks to random noise fluctuations in the data while, if it is too large, it will not fit potential signals or flares. Therefore, it must be calibrated before the BBA can be used in this analysis.

#### 4.3. Calibrating the BBA

To calibrate the BBA, we perform Monte Carlo (MC) simulations by first generating fake light curves and fitting the BBA to them. The light curves are generated by first splitting the 2.0 and 3.0 daily map data sets into declination and right ascension bands. There are four declination bands, centered on [5, 15, 25, 35] degrees, and each being 10 degrees wide. These declination values were selected as HAWC is most sensitive to overhead events (declination=19 deg). There are 36 right ascension bands, centered on [5, 15, ..., 355] degrees. Next, for each declination band, 36 ROIs are defined, each centered on a right ascension band. Each ROI has a radius of 1.44°. This radius was determined by finding the median radius of the IceCube alerts used in this analysis.

With the ROIs defined, the maximum flux search is run for each ROI for each declination band. A distribution of the maximum flux values, created by concatenating all the maximum flux values and associated uncertainties for each ROI, is created. Fake light curves are generated by randomly sampling the flux distribution and its associated uncertainty to create a light curve with 3000 flux values.

Once one fake light curve is generated, it is fit to the BBA with a variable value for the  $ncp\_prior$ . The  $ncp\_prior$  values range from 1.0 to 7.0 (more sensitive to less sensitive), with steps of 0.25. This gives a wide range of values that can be tested quickly, as finer steps sizes greatly increase computation time. For every  $ncp\_prior$  value, 1000 light curves (trials) are generated and then fit. After each run, the change point number  $n_{cp}$  is stored to determine how many blocks were fit to the fake light curve. At the end of the 1000 trials, the mean  $n_{cp}$  is computed to get a False Positive Rate (FPR), defined as having  $n_{cp} > 0$ . The  $ncp\_prior$  values are scanned to achieve a FPR of 5%. This process is repeated 10 times to test the stability of the 5% FPR  $ncp\_prior$  value. The results of the 10 trials for both 2.0 and 3.0 maps are given in Figure 3. The  $ncp\_prior$  values found using this method are 3.6 and 5.9 for the 2.0 and 3.0 maps, respectively.

These two values indicate that the 2.0 maps are more sensitive than the 3.0 maps due to the smaller  $ncp\_prior$  (see Section 2.7 in J. D. Scargle et al. (2013) for details). This is expected due to the spectral assumption made for both; the 2.0 index weights higher energy events more

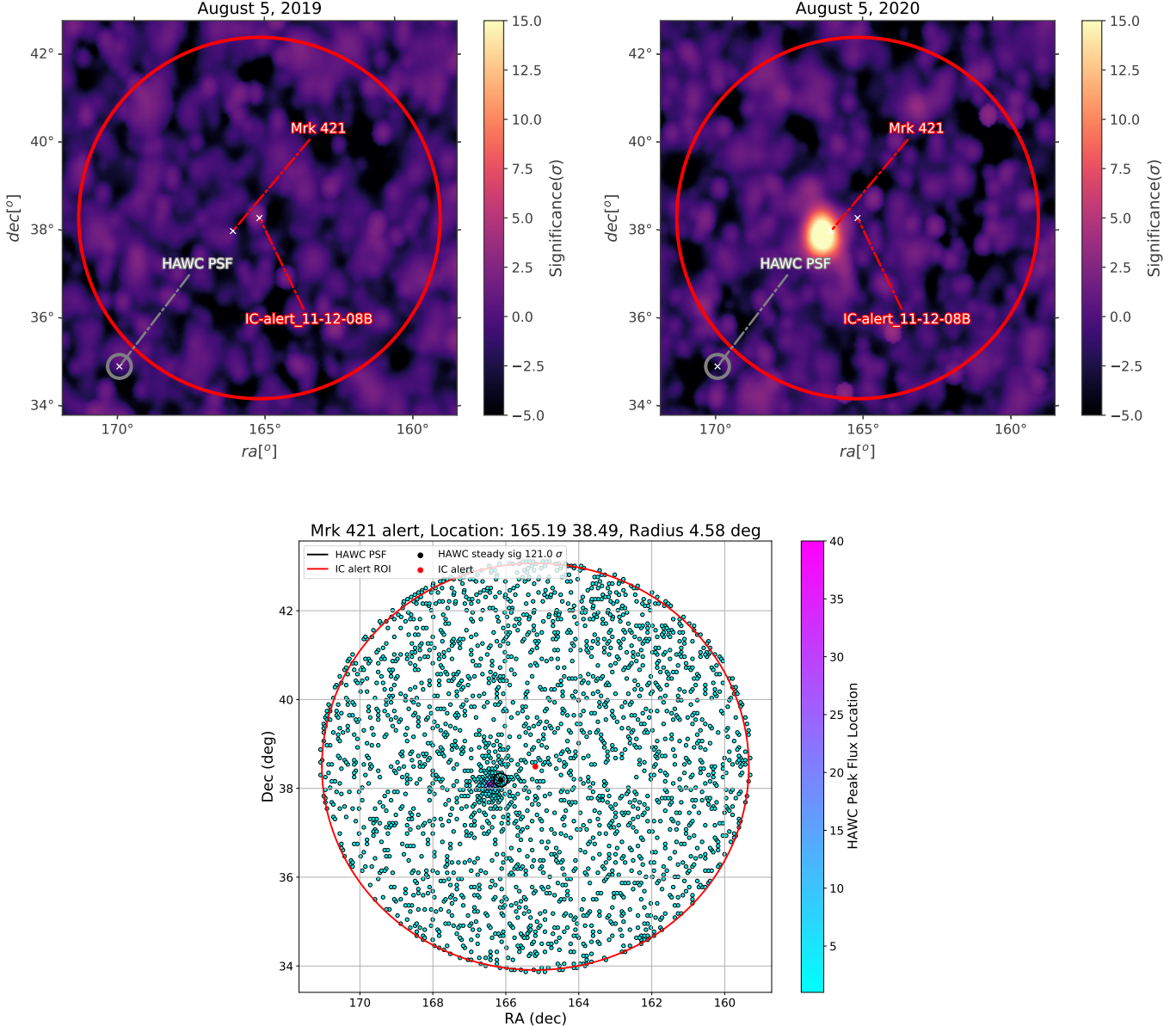


**Figure 2.** The top two plots indicate two daily maps of Mrk 421, one where it is quiet (LEFT) and when it is flaring (RIGHT). The red circle indicates the IceCube alert’s ROI. HAWC’s PSF is indicated in black. The bottom plot shows the frequency that a given RA, Dec has the max flux in the daily map. For a recurrent flaring source like Mrk 421. HAWC sees Mrk 421 to  $121\sigma$  with the Pass 5 time-integrated data.

significantly (A. Albert et al. 2024). Meanwhile, the 3.0 assumption places more weight on those lower energy events, so there is much more data to contend with. In general, the 2.0 maps record lower but more constrained flux values while the 3.0 maps have higher but more uncertain fluxes. This is shown by Figure 6.

## 5. RESULTS

The results for the BBA fits to the HAWC data are presented in Tables 1 and 2 for the 2.0 and 3.0 maps, respectively. The alerts listed in the two tables corre-

spond to “coincident detections”, where the BBA finds a non-null ( $n_{cp} > 0$ ) result for a given alert’s light curve. These coincident detections are purely spatial in nature. None of the detected IceCube alerts have temporal HAWC detections occurring at or near the IceCube alerts. There are 16 (4.3%) and 17 (4.6%) spatial coincident detections for the two maps. This is in line with expected background detection rate of 5%. Of the detected alerts, 3 contained HAWC steady-state  $\sigma > 5$  hotspots in the full 2565-day map. This is in contrast

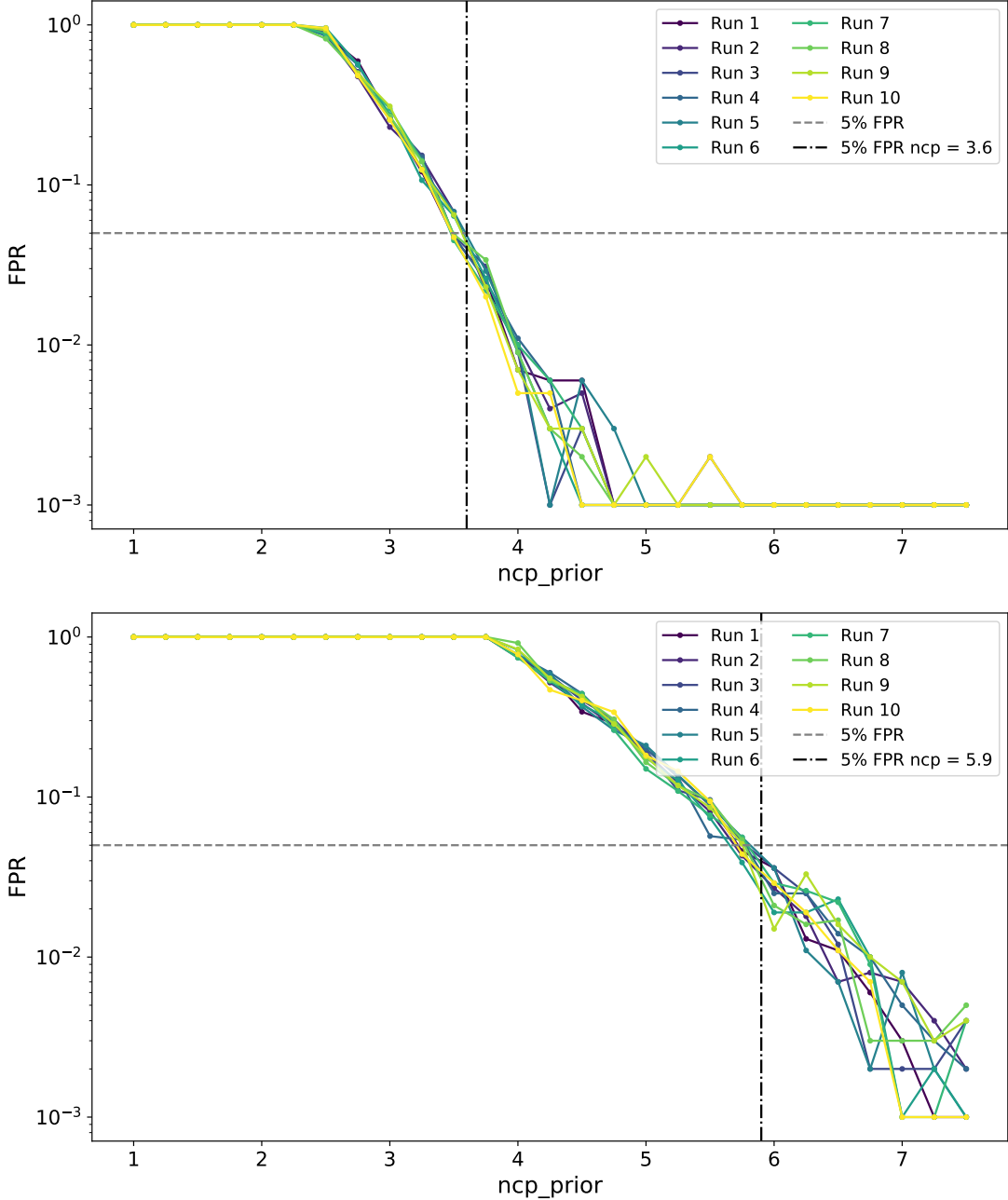


**Figure 3.** The results for the 10 calibrations runs for 2.0 (upper) and 3.0 (lower). For low  $ncp\_prior$  values, both index fits return over a 100% FPR, which is floored to 1. As the  $ncp\_prior$  increases, the FPR decreases until it crosses the 0.05 threshold, indicated by the dashed horizontal line. The value where this happens is indicated by the vertical dashed line and is 3.6 for the 2.0 maps and 5.9 for the 3.0 maps. If the FPR gets below 0.001, it is set to 0.001 for readability.

to the results found in R. Abbasi et al. (2023b), where 8 3HWC sources are found. This is because these authors scanned all IceCube alerts for known sources, while here we only consider the alerts that triggered the BBA. 2 of the 3 detections correspond to the AGNs Mrk 421 and 501 (11-12-08B and 24-03-07G) and are discussed further in Section 6. The third alert, 16-03-07B captures part of the Geminga TeV Halo (A. Albert et al. 2020) at

the edge of its 5.8 degree containment radius. Given the large alert radius and the low probability of  $s = 0.28$ , this is most likely a coincidence. All other detections are possible transient events and are worth investigating.

We consider the 2.0 results first. 14 light curves have only one change point in the BBA analysis, while 2 have greater than 1. These single change point alerts are all located within the first year of HAWC’s operation and

IceCube Alert Parameters					HAWC Results				Nearest $\gamma$ -ray Source
IceCube alert Name	RA (deg)	DEC (deg)	Radius (deg)	$s$	$n_{cp}$	$\sigma_{ss}$	RA (deg)	DEC (deg)	Name (Distance) (deg)
11-12-08B-17:15:15	165.19	38.49	4.58	0.49	61	121	166.16	38.21	Mrk 421 (0.8)
14-05-03B-22:58:06	162.3	46.57	7.17	0.40	1	4.5	166.01	47.46	1ES 1028+511 (5.2)
15-05-26B-00:24:27	139.79	-1.49	1.84	0.28	1	3.2	139.61	-0.82	4FGL J0914.1-0202 (1.4)
15-09-18B-13:05:49	49.83	-2.95	2.23	0.28	1	3.4	49.48	-3.99	—
15-09-23G-00:38:34	103.23	3.96	0.80	0.33	1	2.8	103.8	4.22	—
17-08-19G-06:37:09	26.98	18.88	1.77	0.51	1	3.1	27.42	19.51	—
18-04-10G-18:38:35	218.5	0.56	0.88	0.60	1	2.5	219.42	0.45	—
18-11-21G-13:55:09	132.19	32.93	5.52	0.65	1	4.7	134.08	29.14	RX J0850.5+3455 (2.0)
19-04-13B-15:57:01	245.57	21.98	1.34	0.38	1	3.4	245.65	21.66	—
19-07-30G-20:50:41	226.14	10.77	1.36	0.67	1	3.4	227.29	10.77	PKS 1502+106 (0.3)
21-02-10G-11:53:55	206.06	4.78	0.85	0.65	1	2.1	205.49	5.27	4C +05.57 (0.5)
21-12-16B-07:07:38	316.05	15.79	1.83	0.34	1	2.7	317.64	16.61	4FGL J2100.0+1445 (1.4)
22-05-01B-22:50:58	311.57	18.68	0.93	0.39	1	3.6	311.84	19.12	—
24-02-29B-15:49:06	72.25	15.79	1.14	0.48	1	2.7	72.42	15.68	4FGL J0445.7+1535 (0.8)
24-03-07G-07:45:46	239.63	39.94	15.4	0.61	4	26.1	253.54	39.75	Mrk 501 (13.9)
25-02-07B-02:07:55	132.93	20.66	1.66	0.46	1	3.6	134.08	19.63	—

**Table 1.** The IceCube alerts and location parameters that were detected with this transient search on the index 2.0 maps are given in the first 5 columns. The  $s$  value is the astrophysical probability for that alert. The next 4 columns give the change point number found by the BBA, the HAWC max steady-state significance  $\sigma_{ss}$ , and its location. The last column indicates whether a GeV or TeV  $\gamma$ -ray source exists within the alert ROI. These sources are from either from TeVCat (S. P. Wakely & D. Horan 2008) or 4FGL (J. Ballet et al. 2023). These detections correspond to a 4.3% coincident detection rate. All detections with  $n_{cp} = 1$  occur within the first year of HAWC operations and are discussed further in Section 5.

show a transition from higher to lower flux. The higher average flux duration lasts from 100 to 300 days, depending on the alert. Given the common date range, the higher flux is most likely due to detector maintenance and calibration shortly after operations started as construction finished shortly after HAWC came online in March 2015. This is addressed in the full time-integrated data set, but not for the daily maps, hence the discrepancy. An example is shown in the upper panel in Figure 5.

As for the 3.0 results, they broadly do not suffer from the same systematic issue as the 2.0 results. Aside from two, all light curves are fit by at least 2 change points (3 blocks) to the data. These points are scattered across the whole date range (2015-2024), though they are being fit to under rather than the over fluctuations indicative of flares. These points are slightly below the mean flux distribution and are well constrained. An example is shown in the lower figure in Figure 5.

### 5.1. Sensitivity Studies

To test the sensitivity of the BBA, we perform a series of injection tests using one IceCube alert for both index maps. The selected alert is 24-04-24G, located at 327.08, 3.06, with an alert radius of 1.61 degrees. This alert is selected as it had a null detection for both maps. The

light curves for the 2.0 and 3.0 maps are shown in Figure 6.

After selecting the light curve, we injected fake flares of varying fluxes (in Crab units) with durations of 1, 3, 5, and 10 days. The source is injected at date MJD 59000 (May 31, 2020). The flux scaling factor ranges over 0.5 to 2.0, and is multiplied by the daily Crab flux at 7 TeV for the given day. To find what the actual flux value for the Crab would be, we performed 10 Crab fits on the relevant daily maps. These fits assumed a simple power law to match our maps' assumption along with a fixed index (either 2 or 3). The flux normalization and location (RA, DEC) were free for the fit. The days fit were MJDs 59000 to 59009. Once these fluxes are found, they are multiplied by the desired scaling value to get the final scaled flux.

To simulate the fake flares, the Analysis and Event Reconstruction Integrated Environment (AERIE) framework is used. Described in A. Abeysekara et al. (2018), this is a modular framework that HAWC uses for reconstruction and data manipulation. We used AERIE to construct a series of simulated sources inside the IceCube alert's ROI. To simulate the sources, AERIE used the best fit flux value from the Crab fits and then scaled it by the desired fraction of Crab flux. Lastly, the max

IceCube Alert Parameters					HAWC Results				Nearest $\gamma$ -ray Source	
IceCube alert Name	RA (deg)	DEC (deg)	Radius (deg)	$s$	$n_{cp}$	$\sigma_{SS}$	RA (deg)	DEC (deg)	Name (Distance) (deg)	
11-12-08B-17:15:15	165.19	38.49	4.58	0.49	44	121	166.16	38.21	Mrk 421 (0.8)	
12-08-07G-04:58:17	330.07	1.42	0.68	0.74	2	2.1	330.6	1.79	–	
14-01-14B-21:04:09	337.59	0.71	0.83	0.34	1	2.1	337.5	-0.04	PWN J2227+0037 (0.6)	
15-01-20B-23:37:54	95.89	14.13	0.89	0.34	2	4.3	139.92	40.57	–	
16-01-04G-10:39:08	79.41	5.0	0.85	0.57	2	2.5	79.63	4.89	TXS 0513+054 (0.8)	
16-03-07B-16:43:11	91.32	10.47	5.73	0.28	1	5.8	97.16	10.73	NVS J0660015+124344 (2.1)	
16-06-14B-12:37:43	214.76	40.82	3.65	0.41	2	3.8	210.8	42.9	H1426+428 (2.5)	
16-10-01G-10:32:23	192.57	37.12	2.14	0.64	2	3.1	190.77	37.36	Ton 116 (1.6)	
18-04-10G-18:38:35	218.5	0.56	0.88	0.60	2	2.5	219.42	0.45	–	
19-10-01G-20:09:18	313.99	12.79	3.17	0.59	2	2.7	315.83	10.43	PKS 2047+098 (3.1)	
20-01-09G-23:41:39	165.45	11.8	2.62	0.77	2	3.4	167.17	11.15	TXS 1100+122 (0.4)	
20-11-15G-02:07:26	195.12	1.38	1.26	0.46	2	3.4	194.94	2.05	–	
22-09-28B-12:32:38	207.42	10.43	1.42	0.38	2	2.6	206.98	11.53	RX J1351.3+1115 (0.9)	
22-12-24B-00:55:09	335.74	1.42	0.58	0.28	2	2.4	335.35	1.27	4FGL J2223.3+0122 (0.4)	
22-12-29G-07:25:27	31.9	4.18	1.33	0.54	2	2.7	32.39	4.33	–	
23-04-01B-16:14:18	8.17	1.94	3.06	0.27	2	3.3	5.84	2.84	NVS J003007-000008 (2.0)	
24-02-29B-15:49:06	72.25	15.79	1.14	0.48	2	2.7	72.42	15.68	4FGL J0445.7+1535 (0.8)	

**Table 2.** The IceCube alerts and location parameters that were detected with this transient search on the index 3.0 maps are given in the first 5 columns. The  $s$  value is the astrophysical probability for that alert. The next 4 columns give the change point number found by the BBA, the HAWC max steady-state significance  $\sigma_{SS}$ , and its location. The last column indicates whether a GeV or TeV  $\gamma$ -ray source exists within the alert ROI. These sources are from either from TeVCat (S. P. Wakely & D. Horan 2008) or 4FGL (J. Ballet et al. 2023). These detections correspond to a 4.6% coincident detection rate.

Flare Duration –	2.0 Crab Flux Fraction							3.0 Crab Flux Fraction						
	0.5	0.75	1.0	1.25	1.5	1.75	2.0	0.5	0.75	1.0	1.25	1.5	1.75	2.0
1 day	x	x	✓	✓	✓	✓	✓	x	x	x	✓	✓	✓	✓
3 days	x	✓	✓	✓	✓	✓	✓	x	x	x	✓	✓	✓	✓
5 days	x	✓	✓	✓	✓	✓	✓	x	✓	✓	✓	✓	✓	✓
10 days	x	✓	✓	✓	✓	✓	✓	x	✓	✓	✓	✓	✓	✓

**Table 3.** Detection rate of the BBA with the injected maps. For the 2.0 maps, the lower  $ncp\_prior$  allows for faster detection with lower relative flux compared to the 3.0 maps.

flux search described in Section 4.1 is run on the simulated sources to construct the new, simulated light curve.

With the light curve made, the BBA is then fit to determine how sensitive HAWC is to transient events. The results of this are presented in Table 3. While the two maps differ slightly, in general, HAWC would need to observe multi-day events for fluxes less than the Crab. If the event is higher energy, then Crab-like events only need 1 day to be detected in the 2.0 maps while lower energy events require  $1.25 \times$  Crab flux. The key conclusion is that HAWC requires the event to at least be  $0.75 \times$  Crab flux to be detected in either map. Anything dimmer and HAWC cannot detect it at  $3\sigma$ .

## 6. MULTI-MESSENGER ANALYSIS WITH ICECUBE ALERTS

As AGNs have been proven to emit neutrinos (R. Abbasi et al. 2023c) and two of the neutrino alerts include Mrks 421 (11-12-08B) and 501 (24-03-07G) inside their 90% containment radii, we perform an analysis to determine if the Markarians could be the source of the neutrino alerts. Both Markarians were quiescent during these events, so a steady-state emission model is assumed.

While HAWC does have a long-term analysis of the two Markarians (A. Albert et al. 2022), that analysis only used approximately 1000 days of data. For this analysis, we use the 2565-day Pass 5 data set. Additionally, we used the neural network energy estimator

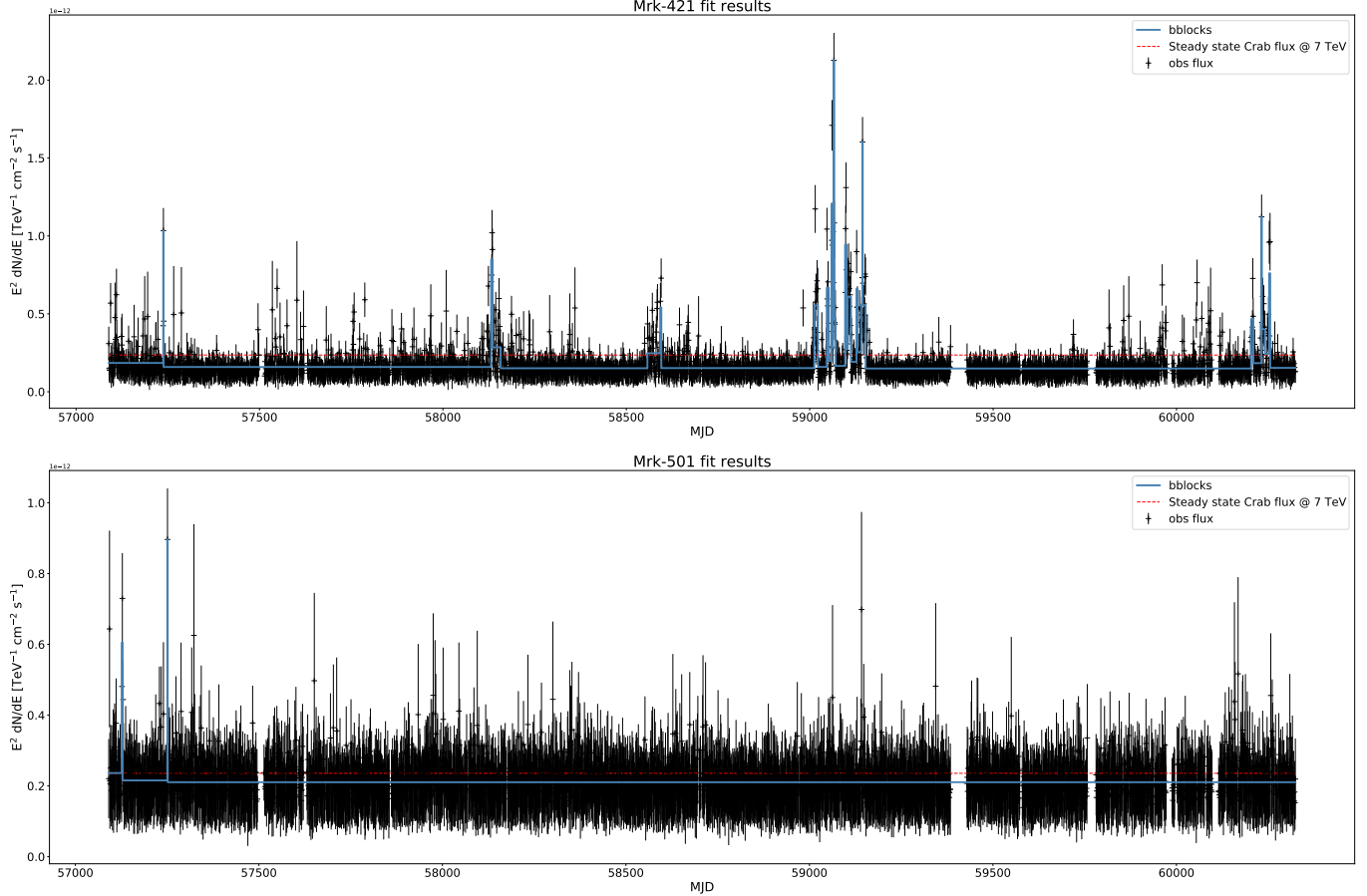


**Figure 4.** The light curves and BBA fits to the HAWC daily light curves for the neutrino alerts containing Mrks 421 (upper plot) and 501 (lower plot). The alerts that captured the two Markarians are 11-12-08B and 24-03-07G, respectively. Mrk 421’s alert occurred before HAWC started operations, and Mrk 501’s alert occurred just after the cut-off for the daily maps. Neither IceCube alert occurred within the data set available for this analysis.

	Mrk 421	Mrk 501
$\sqrt{TS}$	121	26
RA (deg)	$166.14 \pm 0.03$	$253.54 \pm 0.01$
DEC (deg)	$38.19 \pm 0.02$	$39.76 \pm 0.01$
$N_0 [10^{-12} \text{ TeV}^{-1} \text{ cm}^{-2} \text{ s}^{-1}]$	$6.85 \pm 0.23$	$1.07 \pm 0.05$
$\alpha$	$-2.437 \pm 0.027$	$-2.57 \pm 0.05$
$E_c (\text{TeV})$	$9.9 \pm 1.2$	–
$E_{max}$	16.3	15.0

**Table 4.** Fit parameters for the two Markarians. The fits assumed a pivot of 2 TeV. The max energy is presented at the  $2\sigma$  threshold. Additionally, the uncertainties are statistical only.

introduced in Section 3. This data uses a superior background rejection algorithm that are discussed in R. Alfaró et al. (2025b).

To fit the two Markarians, the spectral models from A. Albert et al. (2022) are used. These are a cut-off power law and a power law for Mrks 421 and 501 respectively. Additionally, the Extragalactic Background Light (EBL) must be considered. The EBL absorbs high

energy  $\gamma$ -rays and re-emits them at lower energies. The spectral models fitted for the Markarians are

$$\frac{dE}{dN} = N_o \left( \frac{E}{E_p} \right)^{-\alpha} \times \exp(-\tau(E, z)) \quad (6)$$

and

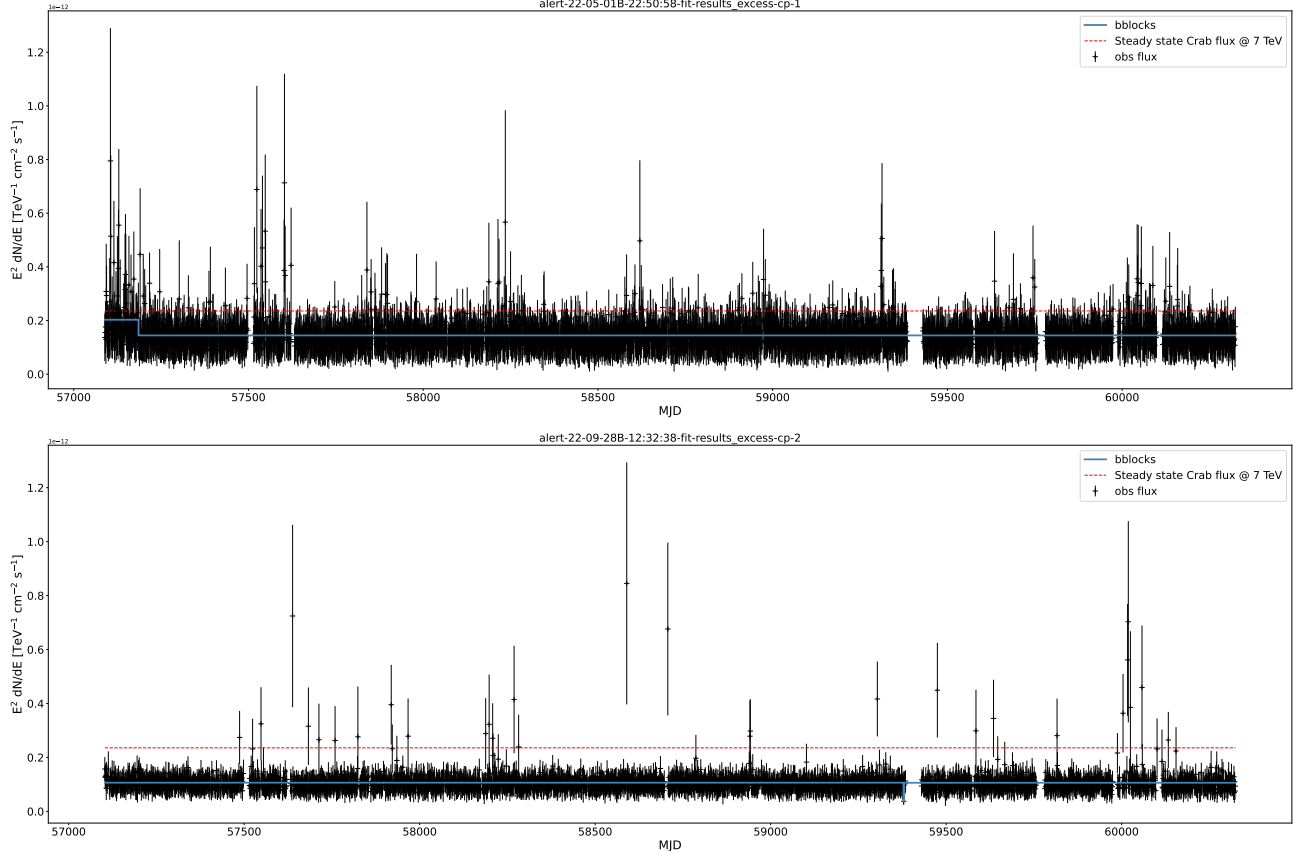


**Figure 5.** Examples of false positives for the 2.0 (upper plot) and 3.0 (lower plot) maps. Aside from the two Markarians, the 2.0 maps all share this slight excess in the first year of data. For the 3.0 maps, there's generally a low flux value around MJD 59400, though it moves slightly, depending on the map.

$$\frac{dE}{dN} = N_o \left( \frac{E}{E_p} \right)^{-\alpha} \times \exp\left(-\frac{E}{E_c}\right) \times \exp(-\tau(E, z)). \quad (7)$$

The pivot energy is fixed to 2 TeV and the EBL model is given by  $-\tau$ . It is a function of the energy and redshift. The model considered is by A. Franceschini et al. (2008) with redshifts of 0.03 and 0.031 for Mrks 421 and 501, respectively (A. Albert et al. 2022). We fit the models using the Multi-Mission Maximum Likelihood (3ML) framework G. Vianello et al. (2015)<sup>34</sup> with the HAWC Accelerated Likelihood (HAL) plugin from Abeysekara et al. (2022)<sup>35</sup>. The results of these fits are given in Table 4 and their spectra are shown in Figure 7.

We then model their emission. As discussed in Section 1, neutrinos are produced via hadronic mechanisms which, at TeV energies, are primarily driven by pion decay. Any  $\gamma$ -rays produced via pion decay will have approximately a 2:1 energy relation with neutrinos (D.

Griffiths 2020). The reported energies of the two neutrinos are 123 and 191 TeV for Mrks 421 and 501, respectively. Therefore, we would expect to see 250 to 400 TeV photons (before EBL attenuation) from the Markarians, making them PeVatrons. It should be noted that multi-wavelength fits for both Mrks 421 and 501 have been described in A. Albert et al. (2022) with a Synchrotron Self-Compton (SSC) leptonic (electron-based) model. This will be discussed later this section.

To test this, the naima (V. Zabalza 2015) and gammamap (A. Donath et al. 2023) python packages are used. Naima is non-thermal modelling framework while gammamap is a flexible fitting package for  $\gamma$ -ray data. We use gammamap to fit a Naima model of pion-producing protons to HAWC data, assuming a cut-off power law spectrum, and consider the EBL attenuation model of  $\gamma$ -rays with the model by A. Franceschini et al. (2008) EBL model.

Fitting this model to the HAWC data provides inconclusive results. The indices and cut-offs are  $-1.23 \pm 0.02$ ,  $250 \pm 5$  TeV for Mrk 421 and  $-0.257 \pm 0.04$ ,  $4600 \pm 910$  TeV for Mrk 501. While the cut-off energies for the fits indicate the Mrks could have produced these neutrinos.

<sup>34</sup> <https://github.com/threeML/threeML>

<sup>35</sup> [https://github.com/threeML/hawc\\_hal](https://github.com/threeML/hawc_hal)

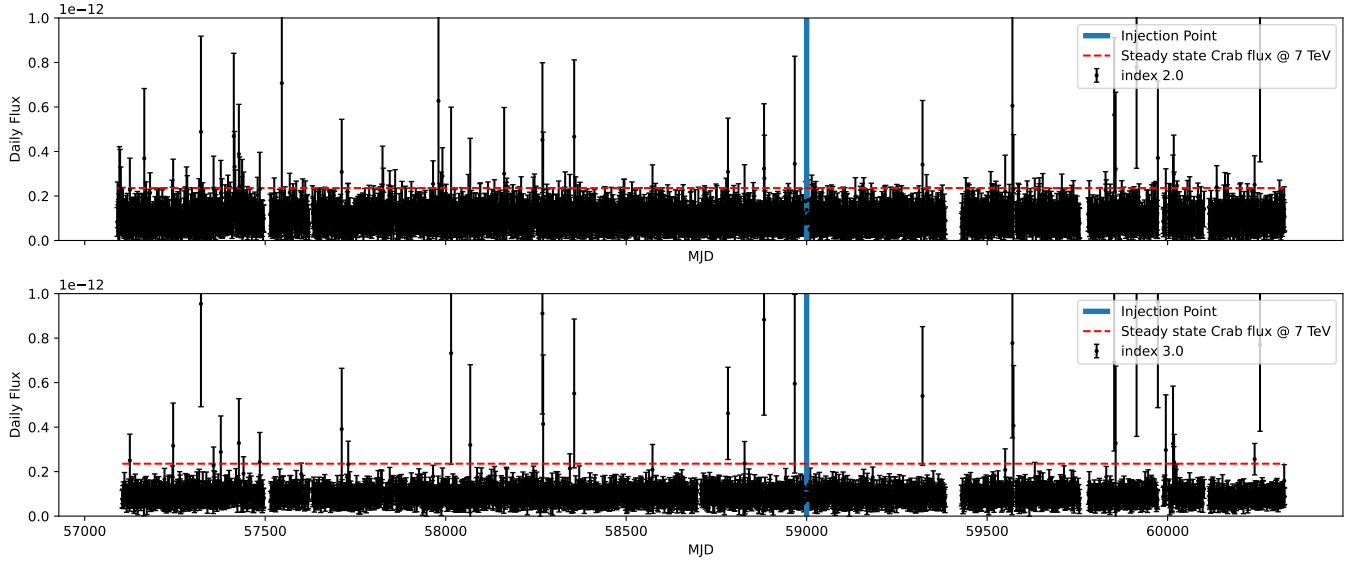


**Figure 6.** Comparing the 2.0 (upper plot) and 3.0 (lower plot) data sets for the IceCube alert 24-04-24G used in the injection studies. The simulated Crab events are injected at MJD 59000, indicated by the vertical blue line.

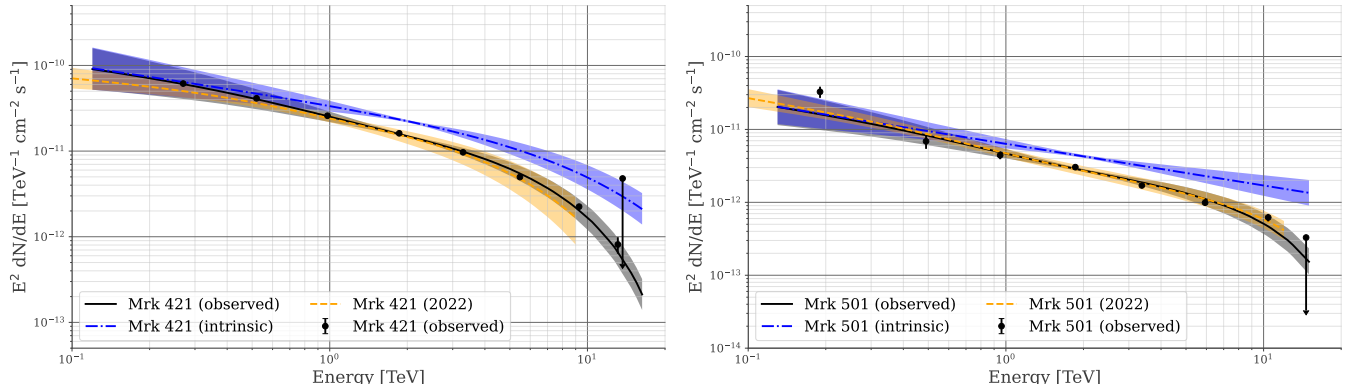


**Figure 7.** The spectral energy distributions for Mrk 421 (right) and Mrk 501 (left). The fits for this work are solid black with their intrinsic spectra indicated in dash dotted blue. Lastly, the orange dashed lines are the previous results from [A. Albert et al. \(2022\)](#).

nos, the highly unphysical nature of the indices indicate unconstrained fits to the data. This is characterized by a reduced  $\chi^2$  value of 0.6 and 0.2 for the two Mrks 421 and 501, respectively. Two potential explanations for the poor quality of the fit results are given below.

The first and more important component is that the preferred particle fitting for Mrks 421 and 501 is the self-scattering Compton model. That is the model used in HAWC's previous results ([A. Albert et al. 2022](#)), and accurately describes all observed data from radio to TeV  $\gamma$ -rays. However, that does not rule out pion decay being present. Certain models, such as a proton-synchrotron model discussed in chapter 10 of [F. A. Aharonian \(2004\)](#), allow for hadronic emission at TeV energies. An alternate option is that the  $\gamma$ -ray data produced from pion

decay gets absorbed by the dense environment in the accretion disk while the neutrinos can easily escape. In this case, the available  $\gamma$ -ray could not be used to model the hadronic process. Testing these scenarios requires further multi-wavelength investigations with more data, which is beyond the scope of this work.

Last of note are the fit results for the pion decay parameters. While the cut-off energies have some promise for producing  $\gamma$ -rays  $> 200$  TeV, the fit values for the indices are not compatible with physical models. Considering the proton-synchrotron model mentioned above, that predicts an index of 2 ([F. A. Aharonian 2004](#)), as does shock acceleration. These poor fit results hint that HAWC's data disfavors a simple pion decay model, though more complex models and external data from

lower energies need to be considered to conclusively rule this out. Lastly, the probabilities for these alerts being astrophysical are 49% for Mrk 421 and 61% for Mrk 501, along with a 90% containment radius of 4.6 and 15.4 degrees respectively. The aforementioned factors further increase the probability of false association.

## 7. SYSTEMATIC UNCERTAINTIES

Considering the HAWC-IceCube coincident search first, there are three factors that affect the results from the BBA: the joint effect of calibration of the BBA and potential declination effects, and a potentially low signal/noise ratio. As the calibration and declination dependence are correlated, they will be considered first. The method used for calibrating the BBA only considered four of the possible 8 declination bands available. These declination bands, centered on [5, 15, 25, 35] degrees, represent the region nearest to HAWC's zenith of 19 degrees. As shown in Figure 3 in [A. Albert et al. \(2024\)](#), HAWC's PSF worsens the further off zenith the events are. This effect is reflected in the average higher flux and larger uncertainty values that can be seen in Mrk 501's light curve in Figure 4. Broadly speaking, alerts closer to zenith have a more constrained uncertainty distribution.

Several methods were tested to address this issue. First, the overall declination range was set to [-20, 60] degrees to help reduce this systematic. Then, several configurations for declination bands were tested. These ranged from 8 bands, each 10 degrees wide, to the 3 bands defined in [A. Albert et al. \(2024\)](#): [0, 26], [26, 37], [37, 46] degrees off zenith. While calibrating these different configurations would succeed, applying them to real alerts usually resulted in unreasonably high detection rates of  $> 10\%$ . A compromise was made to focus on where HAWC is most sensitive while still being able to see a high zenith flare, if it was sufficiently strong. This is the primary reason why most of the detections presented in Tables 1 and 2 are relatively close to HAWC's zenith.

It is also worth noting is that, while the BBA is relatively agnostic to *ncp\_prior* values for moderate to high signal-to-noise ratios, it can have issues in low signal-to-noise environments ([J. D. Scargle et al. 2013](#)). This partially motivated the decision to restrict calibration to HAWC's core declination bands. This decision maximizes the possibility of finding flares within 20 degrees of HAWC's zenith, but penalizes the probability of finding high declination events. Declination-dependent calibration was attempted, but was too inconsistent to be applied across the relevant declination band.

## 8. CONCLUSION

In this analysis, we performed an investigation of public neutrino alerts from IceCube using HAWC. We searched both our 2565-day steady-state and  $\approx 3000$  daily data sets for potential coincidences, either from known  $\gamma$ -ray sources or potential transient events. A Bayesian Block Algorithm was calibrated to fit the maximum flux values collected from the daily maps using regions of interest defined by the 95% containment radius of the IceCube alerts. Two spectral assumptions, 2.0 and 3.0, were used to probe different energy ranges. These achieved a 4.3% and 4.6% coincident detection rate, which is in line with a targeted false positive rate of 5%. We also performed injection studies to determine how sensitive HAWC is to transient events. While brighter (Crab-like) events can be detected in one day, dimmer events need to last multiple days or are impossible to see completely. It is hoped that larger and more powerful observatories like LHAASO and the planned Southern Wide-field Gamma-ray Observatory (SWGO) can significantly improve this search.

Two of these alerts included the active galactic nuclei Markarians 421 and 501, with IceCube recording energies of 123 TeV and 191 TeV, respectively. We investigated whether they could have produced such neutrinos by fitting the two sources with HAWC's Pass 5 data set. The results are inconclusive due to poor constraints placed on the proton distribution, the large containment radii for the two alerts, and the low probability of either alert being astrophysical. With new neutrino observatories like KM3net and P-ONE coming online, neutrino transient events like the IceCube alerts will hopefully become more constrained and point to more neutrino emitters.

## ACKNOWLEDGMENTS

We acknowledge the support from: the US National Science Foundation (NSF); the US Department of Energy Office of High-Energy Physics; the Laboratory Directed Research and Development (LDRD) program of Los Alamos National Laboratory; Consejo Nacional de Ciencia y Tecnología (CONACyT), México, grants LNC-2023-117, 271051, 232656, 260378, 179588, 254964, 258865, 243290, 132197, A1-S-46288, A1-S-22784, CF-2023-I-645, CBF2023-2024-1630, cátedras 873, 1563, 341, 323, Red HAWC, México; DGAPA-UNAM grants IG101323, IG100726, IN111716-3, IN111419, IA102019, IN106521, IN114924, IN110521, IN102223; VIEP-BUAP; PIFI 2012, 2013, PROFOCIE 2014, 2015; the University of Wisconsin Alumni Research Foundation;

the Institute of Geophysics, Planetary Physics, and Signatures at Los Alamos National Laboratory; Polish Science Centre grant, 2024/53/B/ST9/02671; Coordinación de la Investigación Científica de la Universidad Michoacana; Royal Society—Newton Advanced Fellowship 180385; Gobierno de España and European Union-NextGenerationEU, grant CNS2023-144099; The Program Management Unit for Human Resources & Institutional Development, Research and Innovation, NXPO (grant number B16F630069); Coordinación General Académica e Innovación (CGAI-UdeG), PRODEP-

SEP UDG-CA-499; Institute of Cosmic Ray Research (ICRR), University of Tokyo. H.M. acknowledges support under grant number CBF2023-2024-1630. H.F. acknowledges support by NASA under award number 80GSFC21M0002. C.R. acknowledges support from National Research Foundation of Korea (RS-2023-00280210). We also acknowledge the significant contributions over many years of Stefan Westerhoff, Gaurang Yodh and Arnulfo Zepeda Domínguez, all deceased members of the HAWC collaboration. Thanks to Scott Delay, Luciano Díaz and Eduardo Murrieta for technical support.

## REFERENCES

Aartsen, M. G., Ackermann, M., et al. 2018, *Science*, 361, eaat1378

Aartsen, M. G., Ackermann, M., Adams, J., et al. 2017, *Journal of Instrumentation*, 12, P03012

Abbasi, R., Ackermann, M., Adams, J., et al. 2022, *Science*, 378, 538

Abbasi, R., Ackermann, M., Adams, J., et al. 2023a, *Science*, 380, 1338

Abbasi, R., Ackermann, M., Adams, J., et al. 2023b, *The Astrophysical Journal Supplement Series*, 269, 25

Abbasi, R., Ackermann, M., Adams, J., et al. 2023c, *Proceedings of Science*

Abbott, B. P., Abbott, R., Abbott, T. D., et al. 2016, *Physical review letters*, 116, 061102

Abeysekara, et al. 2022, in 37th International Cosmic Ray Conference.

Abeysekara, A., Alfaro, R., Alvarez, C., et al. 2017, *The Astrophysical Journal*, 843, 116

Abeysekara, A., Alfaro, R., Alvarez, C., et al. 2018, *Nuclear Instruments and Methods in Physics Research Section A: Accelerators, Spectrometers, Detectors and Associated Equipment*, 888, 138

Abeysekara, A., Albert, A., Alfaro, R., et al. 2023a, *Nuclear Instruments and Methods in Physics Research Section A: Accelerators, Spectrometers, Detectors and Associated Equipment*, 1052, 168253

Abeysekara, A., Albert, A., Alfaro, R., et al. 2023b, *Nuclear Instruments and Methods in Physics Research Section A: Accelerators, Spectrometers, Detectors and Associated Equipment*, 1052, 168253, doi: <https://doi.org/10.1016/j.nima.2023.168253>

Abreu, P., Albert, A., Alfaro, R., et al. 2019, arXiv preprint arXiv:1907.07737

Aharonian, F. A. 2004, *Very high energy cosmic gamma radiation: a crucial window on the extreme Universe* (World Scientific)

Albert, A., Alfaro, R., Alvarez, C., et al. 2020, *The Astrophysical Journal*, 905, 76

Albert, A., Alfaro, R., Alvarez, C., et al. 2022, *The Astrophysical Journal*, 929, 125

Albert, A., Alfaro, R., Alvarez, C., et al. 2024, *The Astrophysical Journal*, 972, 144

Alfaro, R., Alvarez, C., Anita-Rangel, E., et al. 2025a, arXiv preprint arXiv:2506.16031

Alfaro, R., Alvarez, C., Andrés, A., et al. 2025b, arXiv preprint arXiv:2506.18277

Ballet, J., Bruel, P., Burnett, T., et al. 2023, arXiv preprint arXiv:2307.12546

Cao, Z., della Volpe, D., Liu, S., et al. 2019, arXiv preprint arXiv:1905.02773

Donath, A., Terrier, R., Remy, Q., et al. 2023, *Astronomy & Astrophysics*, 678, A157

Franceschini, A., Rodighiero, G., & Vaccari, M. 2008, *Astronomy & Astrophysics*, 487, 837

Griffiths, D. 2020, *Introduction to elementary particles* (John Wiley & Sons)

Scargle, J. D., Norris, J. P., Jackson, B., & Chiang, J. 2013, *The Astrophysical Journal*, 764, 167

Solares, H. A. A. 2019, *Galaxies*, 7, 19

Vianello, G., et al. 2015, arXiv preprint arXiv:1507.08343

Wagner, S. M., Burd, P. R., Dorner, D., et al. 2021, arXiv preprint arXiv:2110.14797

Wakely, S. P., & Horan, D. 2008, *International Cosmic Ray Conference*, 3, 1341

Wilks, S. S. 1938, *The annals of mathematical statistics*, 9, 60

Zabalza, V. 2015, arXiv preprint arXiv:1509.03319